




RESEARCH ARTICLE

Attenuated brain white matter functional network interactions in Parkinson's disease

Li Meng^{1,2} | Hongyu Wang³ | Ting Zou³ | Xuyang Wang³ | Huafu Chen³  | Fangfang Xie^{1,2}  | Rong Li³ 

¹Department of Radiology, Xiangya Hospital, Central South University, Changsha, People's Republic of China

²National Clinical Research Center for Geriatric Disorders, Xiangya Hospital, Central South University, Changsha, Hunan, China

³The Clinical Hospital of Chengdu Brain Science Institute, MOE Key Laboratory for Neuroinformation, High-Field Magnetic Resonance Brain Imaging Key Laboratory of Sichuan Province, School of Life Science and Technology, University of Electronic Science and Technology of China, Chengdu, People's Republic of China

Correspondence

Rong Li, The Clinical Hospital of Chengdu Brain Science Institute, MOE Key Laboratory for Neuroinformation, High-Field Magnetic Resonance Brain Imaging Key Laboratory of Sichuan Province, School of Life Science and Technology, University of Electronic Science and Technology of China, Chengdu 610054, P.R. China.

Email: rongli1120@gmail.com

Fangfang Xie, Department of Radiology, Xiangya Hospital, Central South University, Changsha 410008, P.R. China.

Email: 76335922@qq.com

Funding information

Chengdu Science and Technology Project, Grant/Award Number: 2021-YF05-01211-SN; National Natural Science Foundation of China, Grant/Award Numbers: 61906034, 62036003, 82072006, U1808204

Abstract

Parkinson's disease (PD) is a neurodegenerative disorder characterized by extensive structural abnormalities in cortical and subcortical brain areas. However, an association between changes in the functional networks in brain white matter (BWM) and Parkinson's symptoms remains unclear. With confirming evidence that resting-state functional magnetic resonance imaging (rs-fMRI) of BWM signals can effectively describe neuronal activity, this study investigated the interactions among BWM functional networks in PD relative to healthy controls (HC). Sixty-eight patients with PD and sixty-three HC underwent rs-fMRI. Twelve BWM functional networks were identified by K-means clustering algorithm, which were further classified as deep, middle, and superficial layers. Network-level interactions were examined via coefficient Granger causality analysis. Compared with the HC, the patients with PD displayed significantly weaker functional interaction strength within the BWM networks, particularly excitatory influences from the superficial to deep networks. The patients also showed significantly weaker inhibitory influences from the deep to superficial networks. Additionally, the sum of the absolutely positive/negative regression coefficients of the tri-layered networks in the patients was lower relative to HC ($p < .05$, corrected for false discovery rate). Moreover, we found the functional interactions involving the deep BWM networks negatively correlated with part III of the Unified Parkinson's Disease Rating Scales and Hamilton Depression Scales. Taken together, we demonstrated attenuated BWM interactions in PD and these abnormalities were associated with clinical motor and nonmotor symptoms. These findings may aid understanding of the neuropathology of PD and its progression throughout the nervous system from the perspective of BWM function.

Abbreviations: BWM, brain white matter; cGCA, coefficient Granger causality analysis; FD, framewise displacement; FDR, false discovery rate; H&Y, Hoehn and Yahr; HAMD, Hamilton Depression Scale; HC, healthy controls; LEDD, levodopa equivalent daily dose; MMSE, Mini-mental State Examination; MNI, Montreal Neurological Institute; MOCA, Montreal Cognitive Assessment; PD, Parkinson's disease; rs-fMRI, resting-state functional magnetic resonance imaging; UPDRS, Unified Parkinson's Disease Rating Scale.

Li Meng and Hongyu Wang contributed equally to this work.

This is an open access article under the terms of the [Creative Commons Attribution-NonCommercial-NoDerivs](https://creativecommons.org/licenses/by-nc-nd/4.0/) License, which permits use and distribution in any medium, provided the original work is properly cited, the use is non-commercial and no modifications or adaptations are made.

© 2022 The Authors. *Human Brain Mapping* published by Wiley Periodicals LLC.

KEYWORDS

Granger causality analysis, interactions, motor and nonmotor symptoms, Parkinson's disease, white matter functional networks

1 | INTRODUCTION

Parkinson's disease (PD) is the second most prevalent neurodegenerative disorder and is characterized by a wide array of motor and non-motor symptoms (Poewe et al., 2017). The main pathological hallmark of PD is Lewy bodies, the widespread accumulation of α -synuclein-immunoreactive inclusions in the nervous system. Studies on neuropathology have revealed that Lewy bodies develop along major fiber pathways, originating in the brain stem before progressing to neocortical regions (Braak et al., 2003). Simultaneously, axonal loss emerges in early stages of the disease, preceding somatic neuronal death and compromising the integrity of the white matter of the brain (brain white matter [BWM]) (Burke & O'Malley, 2013; O'Malley, 2010; Tagliaferro et al., 2015). Thus, investigating BWM is crucial to understanding the pathological mechanisms of PD.

The development of neuroimaging has promoted the study of BWM lesions in PD. Diffusion tensor imaging, commonly used in structural imaging studies, has informed our understanding of the microstructure of BWM lesions in early PD and revealed marked involvement of the genu of the corpus callosum and the superior longitudinal fasciculus. These results suggest alterations in connectivity within frontal and parietal BWM (Bohnen & Albin, 2011; Gattellaro et al., 2009). A study adopting repetitive transcranial magnetic stimulation in combination with diffusion tensor imaging suggested that the structural alignment and cohesion of the superior longitudinal fasciculus tracts may reflect the extent of motor impairments (Rodríguez-Herreros et al., 2015). Structural imaging also revealed that BWM hyperintensities are associated with motor and cognitive symptoms of PD (Bohnen & Albin, 2011; Pavese & Brooks, 2009). However, how BWM function features in PD pathophysiology remains unclear.

There has been increasing interest in applying resting-state functional magnetic resonance imaging (rs-fMRI) to examine BWM neural activation and functional organization (Ding et al., 2013; Huang et al., 2018; M. Li, Newton, et al., 2019; Wu et al., 2017). Studies have verified the intrinsic functional organization of BWM, which manifests as interacting networks of functional modules that can be investigated using rs-fMRI (Fabri & Polonara, 2013; Fabri et al., 2011; Gawryluk et al., 2011; G.-J. Ji et al., 2017; Marussich et al., 2017). Various psychiatric disorders can be characterized by abnormalities in BWM functional activity (Jiang, Luo, et al., 2019; Peer et al., 2017; Zhao et al., 2021). Such abnormalities may have important implications in neurophysiological processes and help explain certain clinical symptoms. Recently, one study examined BWM structural-functional coupling and the abnormalities in PD regarding information transfer with biological networks (i.e., the small-worldness property) (G. J. Ji et al., 2019). While the disruption of gray matter functional network interactions features prominently in PD and is associated with PD symptomatology (Hao et al., 2020; Wang et al., 2022; Wolters

et al., 2019), the interactions among BWM functional networks in patients have not been studied. Since internetwork interactions are basic to the integration of brain function, it is reasonable to speculate that elucidating interactions among BWM functional networks may explain the pathological mechanisms of PD. The Granger causality analysis (GCA) method can be used to uncover the causal relationships among brain regions. The coefficient GCA (cGCA), a type of GCA, can offer insights into the excitatory or inhibitory influences among functional networks via regression coefficients (Chen et al., 2009). Thus, in the present study, the cGCA method was adopted to explore the pathological changes in PD in terms of interactions among BWM functional networks.

The present study illustrates the interactions among BWM functional networks and the corresponding effects on Parkinson's symptoms. The evaluation involved a comparison of 68 patients with PD, relative to 63 healthy individuals (healthy control group, HC). An identified clustering algorithm was conducted within whole-brain white matter to derive 12 functional networks. The interactions among the functional networks were investigated using the cGCA. To further characterize the total influence of each functional network in the interaction model, the causal outflow/inflow strength of each network was examined with a classic graph-theoretic metric. Finally, correlations between interactions and patients' motor and nonmotor symptoms were analyzed. Based on the coupling disturbances of PD's BWM functional network documented in previous studies, we hypothesized that patients with PD would demonstrate disrupted interactions among BWM functional networks, and such disruptions might be associated with the patients' clinical symptoms.

2 | METHODS

2.1 | Subjects

Ninety-two right-handed patients with PD were recruited from the Department of Neurology, Xiangya Hospital of Central South University. The PD diagnosis was made by two or more experienced neurologists based on the criteria of the United Kingdom Parkinson's Disease Society Brain Bank (Hughes et al., 2001). Prior to scanning, the patients completed neurological examinations with a medical interview. The motor features of PD were characterized using the part III of the Unified Parkinson's Disease Rating Scale (UPDRS-III) (Goetz et al., 2008) and Hoehn and Yahr staging (Hoehn & Yahr, 1998), the nonmotor features of PD were evaluated using Mini-mental State Examination (MMSE), Montreal Cognitive Assessment scale (MoCA), and Hamilton Depression Scale (HAMD). Diagnoses ranged from mild to severe Hoehn and Yahr stages of PD (Stages 1–5), wherein a higher score corresponded to a more advanced stage of the disease.

TABLE 1 Clinical and demographic characteristics of subjects

	PD	HC	<i>p</i> value
Subjects, <i>n</i>	68	63	–
Gender, male/female, <i>n/n</i>	37/31	31/32	.5531 ^a
Age, years	47.37 ± 12.03	52.81 ± 10.99	.6076 ^b
Education, years ^c	9.49 ± 3.96	10.33 ± 4.18	.3283 ^d
Duration, years	7.34 ± 5.18	–	–
Onset age, years	47.37 ± 12.03	–	–
Mean FD	0.08 ± 0.05	0.08 ± 0.04	.6390 ^d
MMSE ^c	26.47 ± 3.76	27.07 ± 4.98	.1449 ^b
MOCA ^c	22.64 ± 4.56	23.80 ± 6.06	.0516 ^b
HAMD ^c	7.71 ± 6.86	2.59 ± 2.91	<.0001 ^b
UPDRS-III ^c	33.60 ± 16.86	–	–
H&Y stage	2.49 ± 0.95	–	–
LEDD	411.9 ± 219.9	–	–

Note: Values of variables are presented as mean ± SD.

Abbreviations: FD, framewise displacement; HAMD, Hamilton Depression Scale; H&Y, Hoehn and Yahr; LEDD, levodopa equivalent daily dose; MMSE, Mini-mental State Examination; MOCA, Montreal Cognitive Assessment; UPDRS-III, the part III of the Unified Parkinson's Disease Rating Scale.

^a χ^2 test.

^bNonparametric Mann–Whitney tests.

^cPartial score missed.

^dTwo-sample *t*-tests.

Levodopa equivalent daily dose (LEDD) (Tomlinson et al., 2010) was recorded for each PD patient according to the online Levodopa Equivalent Dose Calculator (<https://www.parkinsonsmeasurement.org/toolBox/levodopaEquivalentDose.htm>). Patients who participated in this study were in an off-medication state after 12 h of withdrawal from dopaminergic drugs. Patients were excluded from the study if they had any of the following: complicated neuropsychiatric disorders such as dementia; head trauma; primary and metastatic tumors; other mental illnesses; any history of drug abuse; or standard contraindications to MRI scanning. In addition, 24 patients were excluded due to incomplete MRI or fMRI scanning (*n* = 13) or excessive head motion (*n* = 11). Ultimately, 68 patients were included for the subsequent analyses.

Sixty-three right-handed healthy individuals were recruited from the local community to comprise the HC group. Imaging data of the subjects were matched by age and gender and quality checked. Subjects' demographics are given in Table 1, and the subject-specific inclusion/exclusion procedure can be found in Section 2.3.

Written informed consent was obtained from all PD patients and HC before the MRI scanning. All examinations were carried out under the guidance of the Declaration of Helsinki 1975. This study was reviewed and approved by the institutional ethics committee of Central South University.

2.2 | Data acquisition

Imaging data were acquired using a 3.0 T GE Signa MR scanner (General Electric Medical Systems) in the Department of Radiology of

Xiangya Hospital of Central South University. High-resolution T1-weighted images were acquired by a three-dimensional fast spoiled gradient-echo sequence (repetition time 7.792 ms; echo time 2.984 ms; flip angle 7°; matrix size 256 × 256; slice thickness 1 mm, no gap; and voxel size 1 mm × 1 mm × 1 mm). Resting-state fMRI images were acquired via a gradient-echo echo-planar imaging sequence (repetition time 2000 ms; echo time 30 ms; flip angle 90°; matrix size 64 × 64; slice thickness 4 mm, 0.6 mm gap; slice number 32; and voxel size 3.44 mm × 3.44 mm × 4.60 mm). The total scan time was 360 s and a total of 180 volumes were collected.

2.3 | Data preprocessing

The fMRI data preprocessing was performed using Data Processing Assistant for Resting-State fMRI (DPARSF v4.3; advanced edition; www.restfmri.net) and Statistical Parametric Mapping toolkits (SPM12; www.fil.ion.ucl.ac.uk/spm). The individual T1 images were segmented into white matter (WM), gray matter, and cerebral spinal fluid (CSF) using SPM12's New Segment algorithm and then normalized to the Montreal Neurological Institute (MNI) template.

During fMRI image preprocessing, the first five volumes were discarded, followed by slice-timing correction, realignment (motion correction cutoff < 3 mm or 3°) to the mean functional image, and coregistration to the anatomical image. Motion spikes were identified using framewise displacement (FD; FD > 0.5 mm) to further minimize motion effects (Power et al., 2012). Meanwhile, subjects with the mean FD bigger than 0.3 mm were excluded from the analyses. Linear detrending was conducted, and nuisance covariates, including

24 motion parameters (Friston et al., 1996) and mean CSF signals, were regressed out. Motion spikes were included as separate regressors to censor the signal at the spike so that correlation values were not further altered (Jiang, Luo, et al., 2019; R. Li et al., 2018). In line with the previous studies (Fan et al., 2020; Peer et al., 2017), temporal band-pass filtering with a frequency range from 0.01 to 0.15 Hz was performed to reduce non-neuronal contributions to blood-oxygen-level-dependent (BOLD) fluctuations. Spatial smoothing (4 mm full-width half-maximum) was implemented on WM functional images, where the WM mask of each subject (identified by co-registering T1 segmentation images to the functional space, threshold set at 0.5) was applied to smoothing (Fan et al., 2020; Peer et al., 2017). Additional threshold of 0.9 was conducted to assess the possible influence of WM probability mask on our results. Finally, the images were normalized to the MNI template and resampled to 3 mm × 3 mm × 3 mm. Six PD patients were excluded for translational or rotational head motion. Five PD patients with larger mean FD > 0.3 mm were discarded. None of the controls exceeded the maximal threshold of translation and maximal rotation or mean FD.

2.4 | White matter functional networks clustering

The clustering analysis on the fMRI data was adapted from the original study by Peer et al. (2017). First, the unified group-level WM masks based on the T1 segmentation results were obtained. Specifically, with the threshold of percentage >60%, voxels in the WM mask averaged across subjects were identified as a group WM mask. To further correct for the deep brain structures (Lorio et al., 2016; Wonderlick et al., 2009), the thalamus, caudate, putamen, globus pallidus, and nucleus accumbens were determined based on the Harvard-Oxford Atlas (Desikan et al., 2006) and removed from the group WM mask. The resulting group WM mask, which included 19,543 voxels, was co-registered to the functional space and resampled at the same voxel size as fMRI images.

BWM functional networks were generated by applying K-means clustering to the group mean Pearson's correlation matrix. Specifically, correlation matrices were first obtained for each subject by calculating the correlation between each BWM voxel and the voxels in the group WM mask, which were subsampled from 19,543 voxels to 4873 nodes based on an interchanging grid strategy (Craddock et al., 2012; Thomas Yeo et al., 2011). The individual correlation matrixes were then averaged across subjects to yield a group mean correlation matrix, which was subjected to K-means clustering.

To evaluate the stability of the number of networks, clusters ranging from 2 to 22 (Lange et al., 2004; Thomas Yeo et al., 2011) were measured and the connectivity matrix was randomly divided into four folds (19,543 × 1218 per fold), after which clustering was performed separately on each fold. To determine the similarity between the clustering results from each fold, adjacency matrices were calculated between any two folds and compared via Dice's coefficient. The averaged Dice's coefficient was used to evaluate the stability of the cluster number (Jiang, Song, et al., 2019; Peer et al., 2017).

Based on the Dice's coefficient of clustering solutions, the number of clusters that yielded the most fine-grained and stable BWM functional networks was 12. Similar to past studies (Fan et al., 2020; Peer et al., 2017), each BWM functional network was overlaid on 20 major BWM fiber tracts from the JHU White Matter Tractography Atlas (Hua et al., 2008; Mori et al., 2005) to evaluate the correspondence between networks and tracts. Then, the resulting networks were classified as superficial, middle, and deep layers.

2.5 | Coefficient GCA

To measure signed and directional influences among the 12 BWM functional networks, bivariate cGCA was performed as hemodynamic delay varied from region to region in the BWM (Courtemanche et al., 2018; M. Li, Newton, et al., 2019; Tong et al., 2017). For each functional network, the individual preprocessed blood oxygenation level-dependent fMRI time series was extracted by averaging the time series of all voxels within the network. The GC strength among networks was calculated using REST (v1.8; www.restfmri.net). In accord with previous works (Fan et al., 2020; Liao et al., 2019), the signed strength and direction of the relationship between any two networks were characterized by each regression coefficient. The positive/negative causal coefficients were interpreted as excitatory/inhibitory paths (source activity predicts subsequent increases/decreases in target activity). Finally, a directed asymmetric matrix (12 × 12 regression coefficient matrix) was acquired for each subject. The following in/out strength value as the cGCA graph theoretic (Liao et al., 2011) was used to describe the inflow/outflow influence strengths of each network: Sum of the absolute regression coefficients of a certain network that denote the incoming or outgoing connections of the network, which is the target/source variable to significantly predict other networks.

2.6 | Network statistical analysis

The within-group GC patterns of BWM functional networks were assessed for each directed edge across subjects in each group with one-sample *t*-test. The network-level between-groups difference patterns for each directed edge were obtained using two-sample *t*-tests. The statistical significance was set at $p < .05$ after adjusting for multiple comparisons with false discovery rate (FDR). Gender, age, mean FD, and Euclidean distance between each two networks were controlled for as confounding variables.

As direct correlation at the same timepoint may be disturbed by the spread of hemodynamic effects across time, the BWM functional network is susceptible to influence by Euclidean distance. As a result, the presumedly across-time causality observed may simply be attributed to the disturbance of correlation and spatial distance. According to previous research (J. Li, Biswal, et al., 2019), the spatial distance and functional connectivity in BWM most likely exhibit a nonlinear relationship, and spatial distance does not significantly affect the

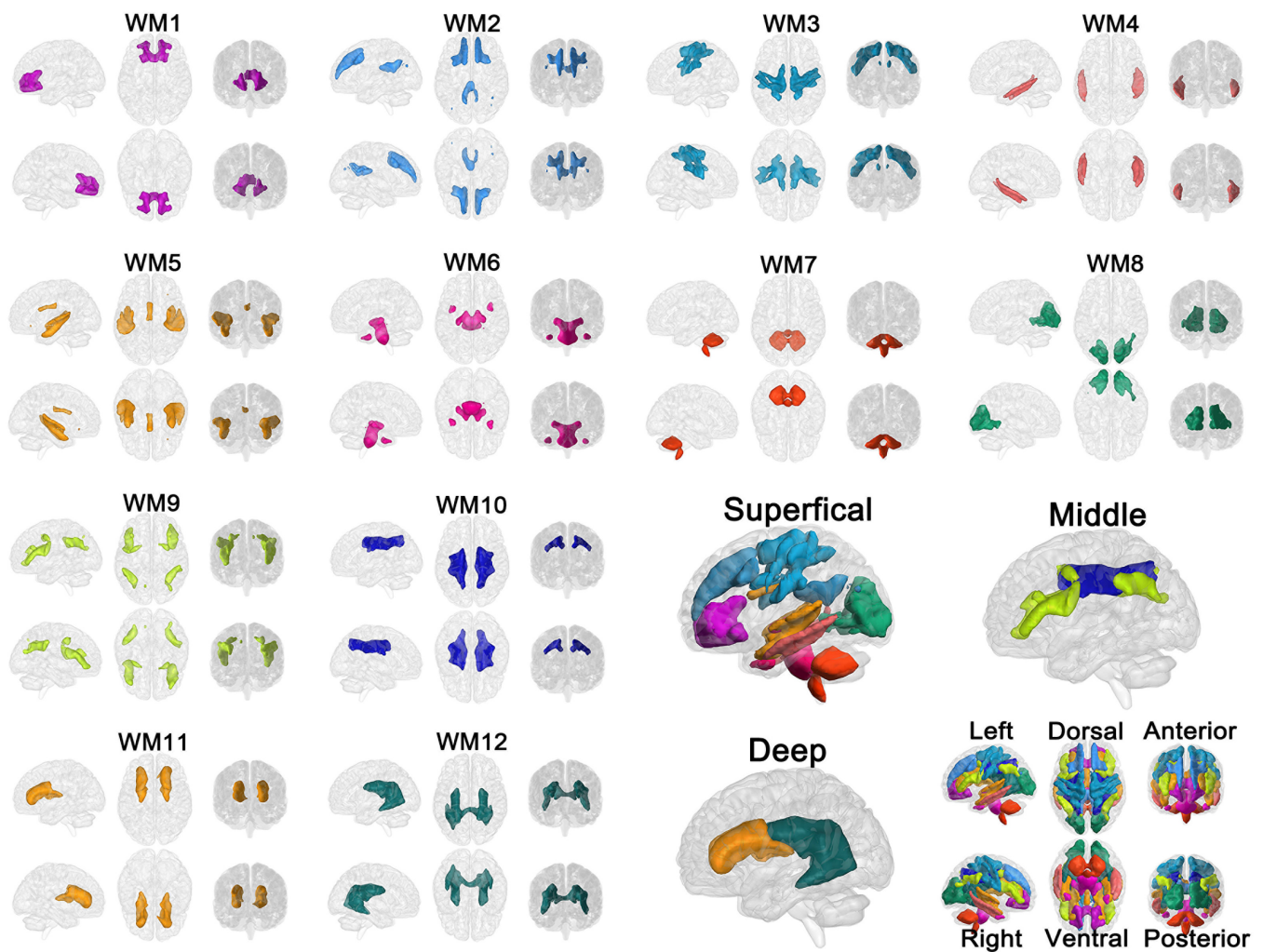


FIGURE 1 Brain white matter functional networks. A total of 12 clusters were identified by K-means clustering algorithm, which can be organized in superficial (WM1-to-WM8), middle (WM9, WM10), and deep (WM11, WM12) layers. WM1, orbitofrontal network; WM2, frontal network; WM3, pre/post-central network; WM4, inferior temporal network; WM5, superior temporal networks; WM6, inferior corticospinal network; WM7, cerebellum network; WM8, occipital network; WM9, anterior/posterior corona radiate network; WM10, superior corona radiate network; WM11, deep frontal network; WM12, deep network

topological properties of BWM functional networks or the nonrandom modular organization. Therefore, Euclidean distances were regressed from the coefficient matrices to exclude spatial effect and correlation disturbance. The Euclidean distance D (in mm) was calculated as the 2-norm ($\|\cdot\|_2$) of any pair of nodal centroids in the MNI space (Mišić et al., 2014; Salvador et al., 2005).

To determine whether the directed edge between each two networks differed from a random result, a permutation test of difference distribution (5000 times) was performed by randomly assigning each subject to one of the two groups corresponding to the size of the original PD and HC groups, respectively, and running a t -test with the same confounding variables (Fan et al., 2020; Liao et al., 2019). The p value was estimated as the percentage of permutations exceeding the actual group difference as calculated in the t -test ($p < .05$, network-based statistic adjusted).

The 12 BWM functional networks were categorized as superficial, middle, and deep network layers. For each subject in the PD and HC

groups, the in/out strength of each layer was computed by summing the absolute strength value of all networks in the layer within the significant group mask. The in/out strength of tri-layer networks in the PD and HC groups was compared via two-sample t -tests ($p < .05$, FDR corrected).

2.7 | Clinical correlation

To explore the associations between GC patterns and motor and non-motor symptoms of PD, Pearson's correlation analyses were performed between altered network influence values and motor/nonmotor scales of PD. In particular, outliers were removed from the scatterplot according to Shepherd's Pi correlation by bootstrapping the Mahalanobis distance (Schwarzkopf et al., 2012). The statistical significance level of the correlation analyses was set as uncorrected $p < .05$.

3 | RESULTS

3.1 | White matter functional networks

The clustering results showed $k = 12$ as the number of clusters that yielded both fine detail and high stability (Dice's coefficient > 0.85). Thus, 12 BWM functional networks were used in the subsequent analysis. The 12 networks were named based on their spatial locations, as follows. WM1, WM2, and WM3 are, respectively, the orbitofrontal, frontal, and pre/post-central networks. WM4 and WM5 are the inferior and superior temporal networks. WM6, WM7, and WM8 are the inferior corticospinal, cerebellum, and occipital networks. WM9 and WM10 represent the anterior/posterior and superior corona radiate networks. Finally, WM11 and WM12 are the deep frontal and deep networks. Corroborating a previous study (Peer et al., 2017), a symmetrical, interlaced pattern of functional networks was identified within the tri-layer BWM via K-means clustering (Figure 1). WM1-to-WM8 are superficial; WM9 are WM10 are middle; and WM11 and WM12 are deep networks. The white matter network-tract correspondence of each network is provided in Table S1.

superior temporal networks. WM6, WM7, and WM8 are the inferior corticospinal, cerebellum, and occipital networks. WM9 and WM10 represent the anterior/posterior and superior corona radiate networks. Finally, WM11 and WM12 are the deep frontal and deep networks. Corroborating a previous study (Peer et al., 2017), a symmetrical, interlaced pattern of functional networks was identified within the tri-layer BWM via K-means clustering (Figure 1). WM1-to-WM8 are superficial; WM9 are WM10 are middle; and WM11 and WM12 are deep networks. The white matter network-tract correspondence of each network is provided in Table S1.

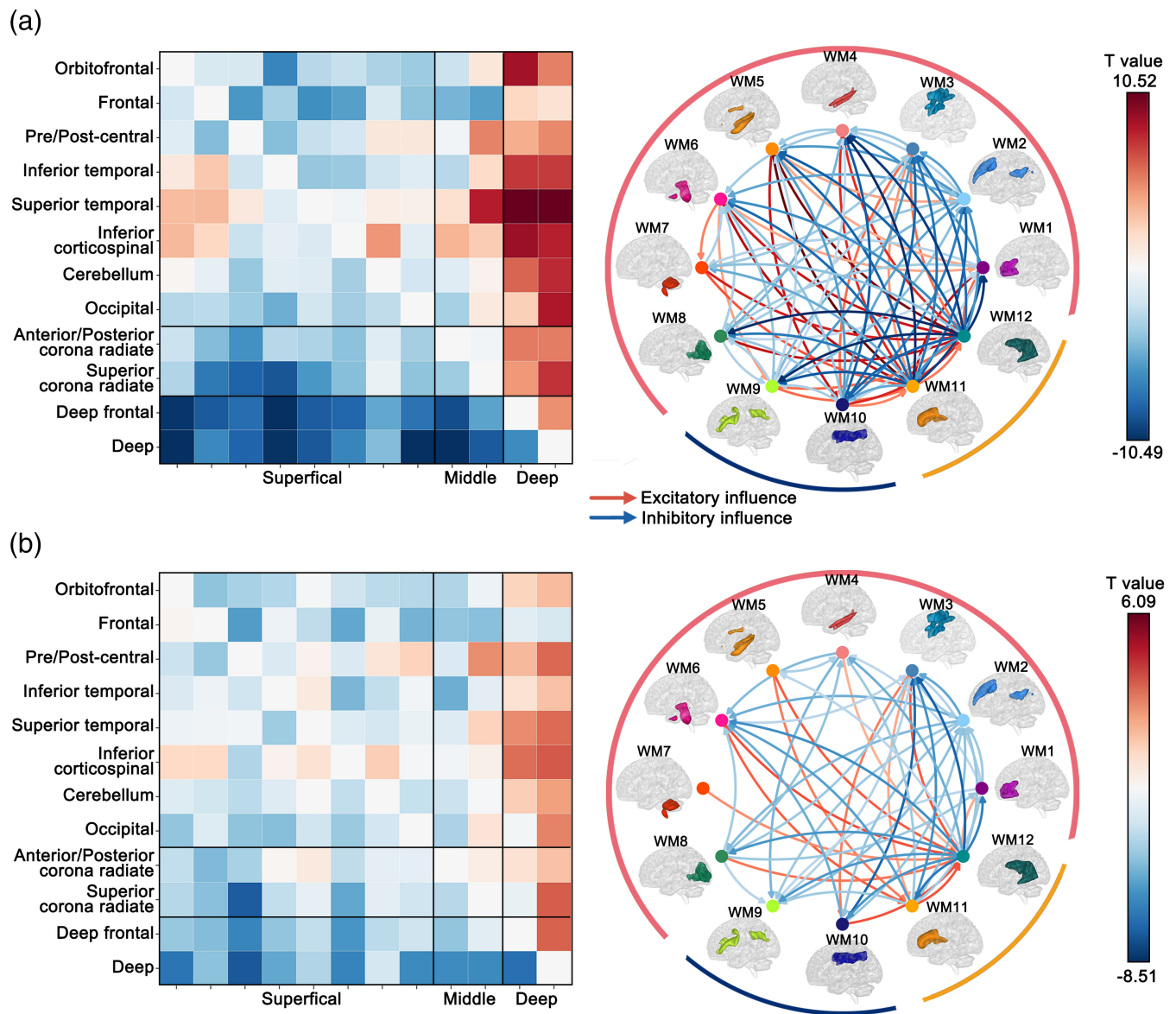


FIGURE 2 Within-group white matter functional networks causal influence patterns across PD ($n = 68$) and HC ($n = 63$) determined by the one-sample t -test ($p < .05$, FDR corrected). Details of the one-sample t -test matrix are shown on the left, where positive/negative t -values denote excitatory or inhibitory influence, respectively. In the Circos figure on the right, red lines represent significant excitatory influence while blue ones represent significant inhibitory influence. The color value of each line becomes darker with the strength of the connection. (a) Within-group white matter functional network interactions in HC. (b) Within-group white matter functional network interactions in PD

Between-group differences in excitatory and inhibitory interactions

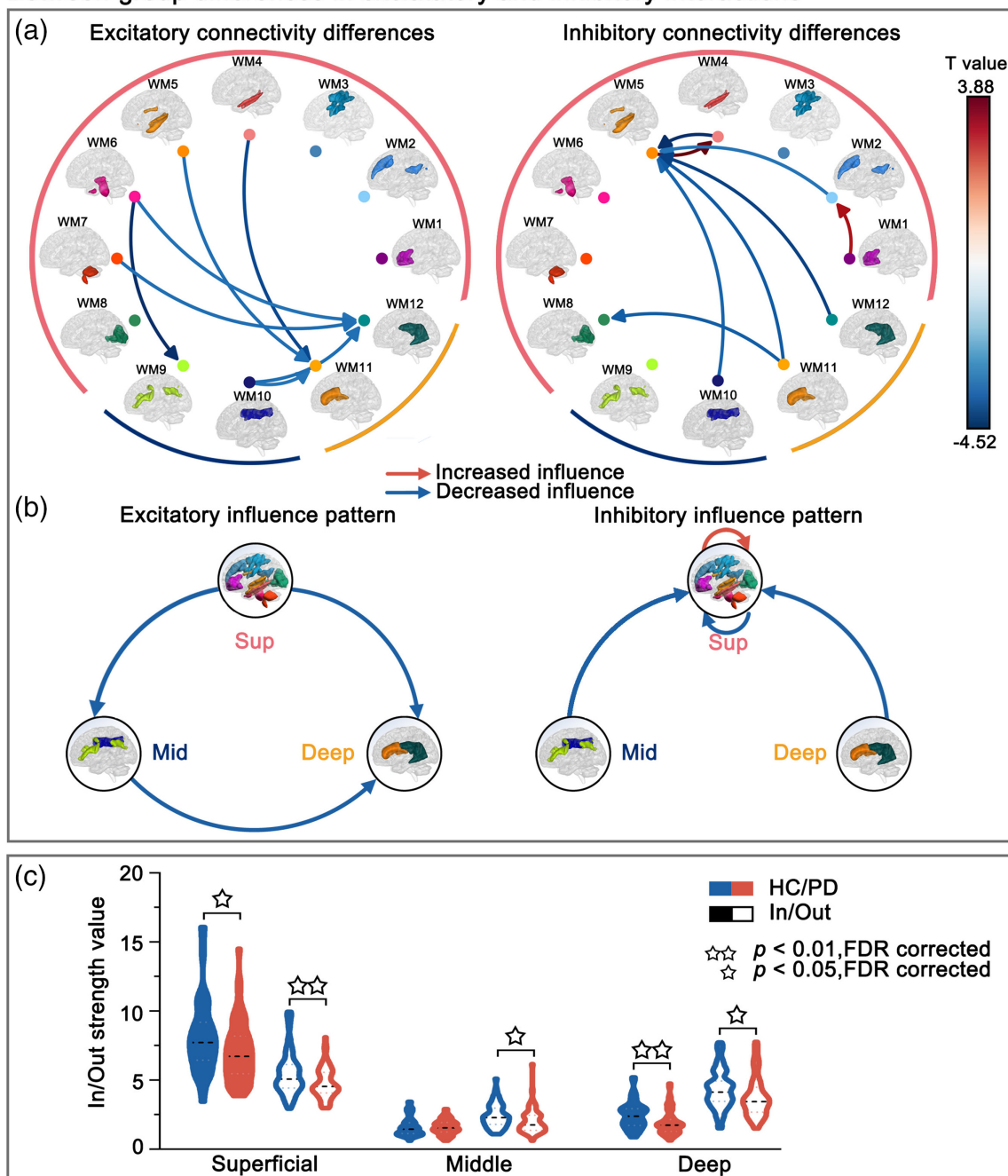


FIGURE 3 Between-group differences in white matter functional networks causal influence determined by two-sample t -test ($p < .05$, FDR corrected). In the figure, two stars denote $p < .01$ and one star denotes $p < .05$. Warm lines denote significantly greater influence; cold lines denote significantly less influence, relative to the HC. The color value of each line becomes darker with the strength of the connection differences. (a) Details of the two-sample t -test are shown in the directed connection differences Circos. (b) Interaction pattern diagram: Compared with HC subjects, in excitatory interaction difference patterns, PD showed significantly lower influence from the superficial \rightarrow deep network, from the superficial \rightarrow middle network and from the middle \rightarrow deep network; in inhibitory interaction differences pattern, PD showed significantly lower influence from the deep \rightarrow superficial network, from the middle \rightarrow superficial network, from the superficial \rightarrow superficial network and showed significant greater influence from the superficial \rightarrow superficial network. (c) The out strength of the superficial network ($T = -2.38$, $p = .019$) and deep network ($T = -2.43$, $p = .016$) was significantly lower in the PD compared with the HC. Additionally, the in strength of the superficial network ($T = -2.54$, $p = .012$) and deep network ($T = -3.41$, $p = .0009$) was significantly lower in the PD.

3.2 | Within-group GC patterns

Within-group BWM functional network influence patterns (Figure 2) across the PD and HC groups were evaluated by one-sample t -test

($p < .05$, FDR corrected). Larger total excitatory and inhibitory influence strengths were found in the deep networks (i.e., deep frontal and deep, WM11 and WM12) compared with the other networks. Similar BWM functional network interactions within PD and HC were

obtained using a relative high threshold of 0.9 for WM probability map (see Figure S1). This partially agrees with previously reported unique features in the deep network (Fan et al., 2020; Jiang, Luo, et al., 2019; Peer et al., 2017). In the Circos figure of PD, a sparser pattern of effective connections can be observed in PD compared with the HC (Figure 3a).

3.3 | Between-group GC patterns

Differences in GC patterns are summarized as the following tri-layer network-level results (Figure 3, Table 2). Compared with HC (Figure 3a,b), in terms of difference patterns in excitatory interactions, PD showed significantly less influence from: the superficial → deep network (WM4 → WM11, $T = -4.09$, $p = .00008$; WM5 → WM11, $T = -3.42$, $p = .0009$; WM6 → WM12, $T = -3.35$, $p = .001$; WM7 → WM12, $T = -3.41$, $p = .0008$); from the superficial → middle network (WM6 → WM10, $T = -4.52$, $p = .00001$); and from the middle → deep network (WM10 → WM11, $T = -3.29$, $p = .0013$; WM10 → WM12, $T = -3.39$, $p = .0009$). In terms of difference patterns in inhibitory interactions, PD showed significantly less influence than did the HC group from: the deep → superficial network (WM11 → WM5, $T = -3.58$, $p = .0005$; WM11 → WM8, $T = -3.53$, $p = .0006$; WM12 → WM5, $T = -4.0$, $p = .0001$); from the middle → superficial network (WM10 → WM5, $T = -3.42$, $p = .0008$); and from the superficial → superficial network (WM2 → WM5, $T = -3.14$, $p = .0021$; WM4 → WM5, $T = -4.30$, $p = .00003$). PD showed significantly greater influence than did the HC group from the superficial → superficial network (WM1 → WM2, $T = 3.31$, $p = .0012$; WM5 → WM4, $T = 3.88$, $p = .0002$).

GC pattern	Layer	Network	T value	p value
Excitatory	Superficial → Deep	WM4 → WM11	-4.09	<.0001
		WM5 → WM11	-3.42	.0009
		WM6 → WM12	-3.35	.0010
		WM7 → WM12	-3.41	.0008
	Superficial → Middle	WM6 → WM10	-4.52	<.0001
	Middle → Deep	WM10 → WM11	-3.29	.0013
		WM10 → WM12	-3.39	.0009
Inhibitory	Deep → Superficial	WM11 → WM5	-3.58	.0005
		WM11 → WM8	-3.53	.0006
		WM12 → WM5	-4.00	.0001
	Middle → Superficial	WM10 → WM5	-3.42	.0008
		Superficial → Superficial	WM2 → WM5	-3.14
	WM4 → WM5		-4.30	<.0001
	WM1 → WM2		3.31	.0012
	WM5 → WM4	3.88	.0002	

Note: The statistical significance was set at $p < .05$ after adjusting for multiple comparisons with FDR correction.

Abbreviations: WM1, orbitofrontal network; WM2, frontal network; WM4, inferior temporal network; WM5, superior temporal networks; WM6, inferior corticospinal network; WM7, cerebellum network; WM8, occipital network; WM10, superior corona radiate network; WM11, deep frontal network; WM12, deep network.

Relative to the HC, the out strength of the superficial ($T = -2.98$, $p = .0034$), middle ($T = -2.49$, $p = .0140$), and deep ($T = -2.43$, $p = .0164$) networks was significantly less in the PD group, as was the in strength of the superficial ($T = -2.65$, $p = .0089$) and deep ($T = -3.43$, $p = .0008$) networks (Figure 3c).

We performed additional analysis to verify the main findings. To investigate whether the brain atrophy of PD may potentially contribute to the abnormal white matter functional network interactions, we correlated the absolute volumes of the white matter and gray matter with the white matter functional network GC strength of PD, respectively. This analysis did not identify any significant correlation suggesting that abnormalities in the white matter functional network may be unaffected by functional and structural atrophy in PD (Table S2).

3.4 | Clinical correlation results

We found that both the UPDRS-III and HAMD scores correlated with attenuations in network interactions in PD relative to HC. Specifically, the greater the motor symptoms, the more the network interactions were weakened (Figure 4a): WM6 → WM12 influence strength ($r = -.26$, $p = .0356$); WM11 → WM8 influence strength ($r = -.33$, $p = .0064$); WM11 → WM5 influence strength ($r = -.27$, $p = .0329$); and WM4 → WM11 influence strength ($r = -.30$, $p = .0200$). Similarly, the HAMD score negatively correlated with attenuations in network interactions in PD (Figure 4b): WM11 → WM8 influence strength ($r = -.33$, $p = .0172$); WM4 → WM11 influence strength ($r = -.30$, $p = .0300$).

TABLE 2 Between-group differences in white matter functional network interactions between healthy controls and PD patients

4 | DISCUSSION

In this study, 12 BWM functional networks composed of three layers (superficial, middle, and deep) were identified in the PD and HC groups based on whole-brain resting-state correlation matrices. The HC group showed significant and consistent influence strength of excitatory and inhibitory effects in the deep networks, while the

excitability in PD was lower both from the superficial to middle networks and from the middle to deep networks. Additionally, compared with the HC, the inhibition was lower from the middle and deep networks to superficial networks and higher among the superficial networks in PD. Moreover, the in/out strength of the deep and superficial networks was significantly lower in the PD group. Finally, we found the deep BWM networks corresponding to the primary

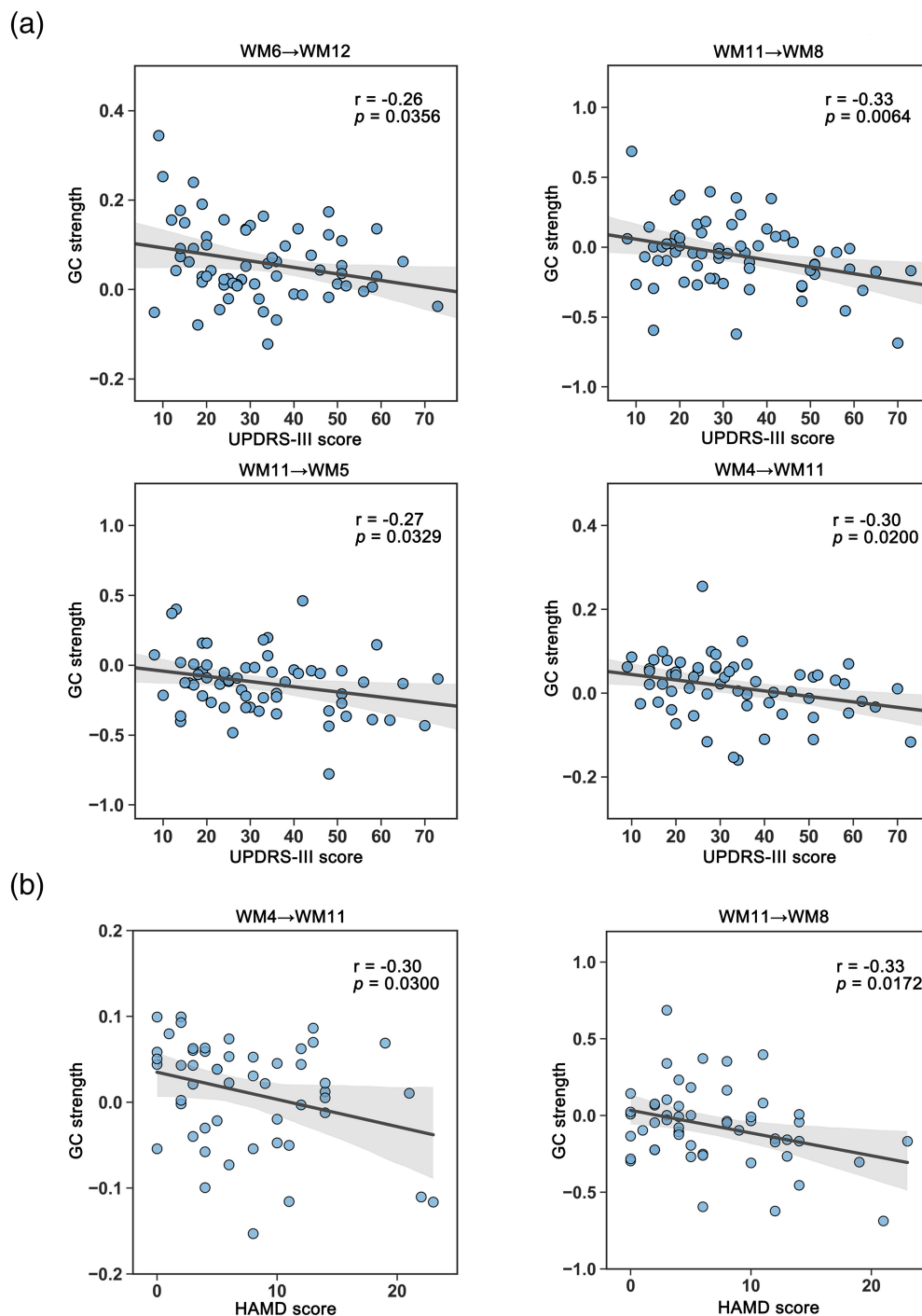


FIGURE 4 The decreases in white matter functional network interactions of PD correlated with the motor/nonmotor symptoms. Significant correlations were identified between GC strengths and (a) UPDRS-III scores and (b) HAMD scores. p was the adjusted p -statistic to account for outlier removal by bootstrapping the Mahalanobis distance. WM4, inferior temporal network; WM5, superior temporal network; WM6, inferior corticospinal network; WM11, deep frontal network; WM12, deep network; UPDRS-III, the part III of the Unified Parkinson's Disease Rating Scale; HAMD, Hamilton Depression Scale. (a) Correlations between white matter functional network interactions and motor symptoms of PD. (b) Correlations between white matter functional network interactions and nonmotor symptoms of PD

fiber tracts (superior longitudinal, forceps minor, and anterior thalamic radiation) showed significant changes that were associated with motor and nonmotor symptoms in PD. To our knowledge, this is the first GCA-based study that explores the interactions between BWM functional networks in PD. Consistent with our hypothesis, patients with PD demonstrated extensive interrupted interactions among the BWM functional networks, and the deep networks possessed distinctive traits that were correlated with PD motor and nonmotor symptoms.

A total of 12 stable BWM functional networks were identified in the current study, which is in accord with the previous studies (Fan et al., 2020; Jiang, Song, et al., 2019; Peer et al., 2017) and adds to the evidence that the study of BWM networks in PD is feasible. The HC group showed significant and consistent influence strength of excitatory and inhibitory effects in the deep networks, indicating that the deep networks are important to BWM function. However, the PD group showed fewer effects of within-group interactions of influence as well as the number of significant connectivity edges, suggesting that the deep networks in PD are disrupted.

The deep networks correspond to the superior longitudinal fasciculus, forceps major, forceps minor, and thalamic radiation tracts, which involve body control, motor ability, and other higher-level functions. Compared with the superficial BWM tracts, the deep networks are less surrounded by gray matter (Costentin et al., 2019; Pietracupa et al., 2018; Sanjari Moghaddam et al., 2020; Wen et al., 2016; Wen et al., 2018). In terms of brain function, in the present study, hardly any correlation pattern was observed between the deep and gray matter networks, which differs from the synchronous neural activity between the superficial BWM networks and cortical gray-matter networks (Ding et al., 2018; Peer et al., 2017). Therefore, there is an anatomical basis for the correlation between abnormal changes in the deep networks and motor symptoms of PD.

This study showed that PD patients exhibited weakened interactions in both excitatory and inhibitory network influences, relative to HC. The interaction between networks is the basis for the integration of brain functions (Park & Friston, 2013), namely the interaction between motor and cognitive brain functions and distributed functional networks. For instance, in schizophrenia, BWM functional networks were classified and abnormalities in spontaneous oscillation and connection with gray matter have been observed (Jiang, Luo, et al., 2019). In terms of PD, subcortical BWM lesions were associated with more severe gait symptoms and rigidity (Bohnen & Albin, 2011). The abovementioned pattern of inhibitory interactions may arise from a drop in dopaminergic transmission in the motor region of the striatum, leading to lower excitatory interactions. Impairment of the deep and middle network interactions, which leads to disrupted communication with the superficial networks, may explain the motor impairments and cognitive dysfunction. The present results revealed the disrupted excitatory and inhibitory interaction patterns of tri-layer BWM functional networks at the whole-brain network scale in PD, which further illustrates the functional activity changes in motor and nonmotor circuits.

The significantly weakened excitatory influence from the inferior corticospinal network to the deep network, excitatory influence from the inferior temporal network to the frontal deep network, as well as the significantly weakened inhibitory influence from the frontal deep network to the visual network in PD patients were found to be negatively correlated with the UPDRS-III and HAMD scores. In other words, greater PD motor and nonmotor symptoms were associated with greater attenuation in the network interactions relative to HC. The tracts involved in these BWM functional networks are associated with motor and cognition functions physiologically. Specifically, cortical areas including the primary motor cortex, supplementary motor area, and premotor cortex project to the spinal cord through the corticospinal tract, a critical channel that involves the cortico-basal ganglia-thalamo-cortical network affected by PD (Burciu & Vaillancourt, 2018). In addition, the basal ganglia network is composed of intricately interconnected subcortical nuclei that are involved in cognition, motor control, and motivation (Lanciego et al., 2012). The loss of dopaminergic cells in the substantia nigra pars compacta is considered the underlying mechanism of PD and impairment to the projecting axons of neurons in the substantia nigra are seen in early stages of PD. These axons are intimately connected to the BWM of the deep networks, and we therefore speculate that the combination of changes in the deep networks and basal ganglia-thalamo loop lead to the motor and nonmotor symptoms of PD. A recent transcranial magnetic stimulation (TMS) study showed the fractional anisotropy of the tract from supplementary motor area to globus pallidus was predictive to the treatment effect of TMS (G. J. Ji et al., 2021), providing a structural basis for our finding that changes in the deep network are associated with clinical motor symptoms of PD. Future studies that explore the relationships between BWM function and clinical outcomes of TMS or deep-brain stimulation treatment may offer novel applicable neuromarkers for PD clinical realm.

Despite our findings, this study has limitations in the following aspects. First, sub-scores for tremor, rigidity, bradykinesia, and posture were not included in our data, so a more specific assessment of the association between these subdivided motor symptoms and BWM function was not possible. In future studies, we will take these into account and consider specific features, such as freezing gait, in more detail. Second, the long-term effect of medication may persist in patients even if assessed in a medication-off state. Finally, this is a single-center study with a limited sample size; future studies should enroll more subjects to validate the stability of results.

This work elucidates the pathological changes of PD regarding BWM functional network interactions. It was found that the BWM networks associated with deep structural tracts have extensive abnormal interactions with superficial and middle networks in PD. Furthermore, the attenuated interactions of the deep networks were significantly associated with motor and nonmotor symptoms in PD. These findings suggest that the communication functions between BWM networks are impaired and these abnormalities may exacerbate or contribute to some motor and cognitive deficits

associated with PD. Our study provides novel insights into the neuropathology of PD from the perspective of BWM function.

ACKNOWLEDGMENTS

This work was supported by the National Natural Science Foundation of China (Nos. 82072006, 62036003, 61906034, and U1808204), and the Chengdu Science and Technology Project (2021-YF05-01211-SN).

CONFLICT OF INTEREST

The authors declare no competing financial interests.

DATA AVAILABILITY STATEMENT

All primary data and code used for the analysis are available from the corresponding author on reasonable request. Data for the Parkinson's disease patients and healthy controls as well as any specialized codes generated for this study are available from the corresponding author on reasonable request.

ORCID

Huafu Chen  <https://orcid.org/0000-0002-4062-4753>

Fangfang Xie  <https://orcid.org/0000-0003-2575-0425>

Rong Li  <https://orcid.org/0000-0001-7266-0241>

REFERENCES

- Bohnen, N. I., & Albin, R. L. (2011). White matter lesions in Parkinson disease. *Nature Reviews Neurology*, 7(4), 229–236.
- Braak, H., Del Tredici, K., Rüb, U., De Vos, R. A., Steur, E. N. J., & Braak, E. (2003). Staging of brain pathology related to sporadic Parkinson's disease. *Neurobiology of Aging*, 24(2), 197–211.
- Burciu, R. G., & Vaillancourt, D. E. (2018). Imaging of motor cortex physiology in Parkinson's disease. *Movement Disorders*, 33(11), 1688–1699. <https://doi.org/10.1002/mds.102>
- Burke, R. E., & O'Malley, K. (2013). Axon degeneration in Parkinson's disease. *Experimental Neurology*, 246, 72–83. <https://doi.org/10.1016/j.expneurol.2012.01.011>
- Chen, G., Hamilton, J. P., Thomason, M. E., Gotlib, I. H., Saad, Z. S., & Cox, R. W. (2009). Granger causality via vector auto-regression tuned for fMRI data analysis. *Proceedings of the International Society for Magnetic Resonance in Medicine*, 17, 1718.
- Costentin, G., Derrey, S., Gérardin, E., Cruypheninck, Y., Pressat-Laffouilhère, T., Anouar, Y., Wallon, D., le Goff, F., Welter, M. L., & Maltête, D. (2019). White matter tracts lesions and decline of verbal fluency after deep brain stimulation in Parkinson's disease. *Human Brain Mapping*, 40(9), 2561–2570. <https://doi.org/10.1002/hbm.24544>
- Courtemanche, M. J., Sparrey, C. J., Song, X., MacKay, A., & D'Arcy, R. C. (2018). Detecting white matter activity using conventional 3 tesla fMRI: An evaluation of standard field strength and hemodynamic response function. *NeuroImage*, 169, 145–150.
- Craddock, R. C., James, G. A., Holtzheimer, P. E., Hu, X. P., & Mayberg, H. S. (2012). A whole brain fMRI atlas generated via spatially constrained spectral clustering. *Human Brain Mapping*, 33(8), 1914–1928. <https://doi.org/10.1002/hbm.21333>
- Desikan, R. S., Ségonne, F., Fischl, B., Quinn, B. T., Dickerson, B. C., Blacker, D., Buckner, R. L., Dale, A. M., Maguire, R. P., Hyman, B. T., Albert, M. S., & Killiany, R. J. (2006). An automated labeling system for subdividing the human cerebral cortex on MRI scans into gyral based regions of interest. *NeuroImage*, 31(3), 968–980.
- Ding, Z., Huang, Y., Bailey, S. K., Gao, Y., Cutting, L. E., Rogers, B. P., Newton, A. T., & Gore, J. C. (2018). Detection of synchronous brain activity in white matter tracts at rest and under functional loading. *Proceedings of the National Academy of Sciences*, 115(3), 595–600. <https://doi.org/10.1073/pnas.1711567115>
- Ding, Z., Newton, A. T., Xu, R., Anderson, A. W., Morgan, V. L., & Gore, J. C. (2013). Spatio-temporal correlation tensors reveal functional structure in human brain. *PLoS One*, 8(12), e82107.
- Fabri, M., & Polonara, G. (2013). Functional topography of human corpus callosum: An fMRI mapping study. *Neural Plasticity*, 2013, 1–15.
- Fabri, M., Polonara, G., Mascioli, G., Salvolini, U., & Manzoni, T. (2011). Topographical organization of human corpus callosum: An fMRI mapping study. *Brain Research*, 1370, 99–111.
- Fan, Y. S., Li, Z., Duan, X., Xiao, J., Guo, X., Han, S., Guo, J., Yang, S., Li, J., Cui, Q., Liao, W., & Chen, H. (2020). Impaired interactions among white-matter functional networks in antipsychotic-naïve first-episode schizophrenia. *Human Brain Mapping*, 41(1), 230–240. <https://doi.org/10.1002/hbm.24801>
- Friston, K. J., Williams, S., Howard, R., Frackowiak, R. S., & Turner, R. (1996). Movement-related effects in fMRI time-series. *Magnetic Resonance in Medicine*, 35(3), 346–355.
- Gattellaro, G., Minati, L., Grisoli, M., Mariani, C., Carella, F., Osio, M., Ciceri, E., Albanese, A., & Bruzzone, M. G. (2009). White matter involvement in idiopathic Parkinson disease: A diffusion tensor imaging study. *American Journal of Neuroradiology*, 30(6), 1222–1226. <https://doi.org/10.3174/ajnr.A1556>
- Gawryluk, J. R., Mazerolle, E. L., Brewer, K. D., Beyea, S. D., & D'Arcy, R. C. (2011). Investigation of fMRI activation in the internal capsule. *BMC Neuroscience*, 12(1), 1–7.
- Goetz, C. G., Tilley, B. C., Shaftman, S. R., Stebbins, G. T., Fahn, S., Martinez-Martin, P., Poewe, W., Sampaio, C., Stern, M. B., Dodel, R., Dubois, B., Holloway, R., Jankovic, J., Kulisevsky, J., Lang, A. E., Lees, A., Leurgans, S., LeWitt, P. A., Nyenhuis, D., ... LaPelle, N. (2008). Movement Disorder Society-sponsored revision of the unified Parkinson's disease rating scale (MDS-UPDRS): Scale presentation and clinimetric testing results. *Movement Disorders: Official Journal of the Movement Disorder Society*, 23(15), 2129–2170.
- Hao, L., Sheng, Z., Ruijun, W., Kun, H. Z., Peng, Z., & Yu, H. (2020). Altered granger causality connectivity within motor-related regions of patients with Parkinson's disease: A resting-state fMRI study. *Neuroradiology*, 62(1), 63–69.
- Hoehn, M. M., & Yahr, M. D. (1998). Parkinsonism: Onset, progression, and mortality. *Neurology*, 50(2), 318.
- Hua, K., Zhang, J., Wakana, S., Jiang, H., Li, X., Reich, D. S., Calabresi, P. A., Pekar, J. J., van Zijl, P. C. M., & Mori, S. (2008). Tract probability maps in stereotaxic spaces: Analyses of white matter anatomy and tract-specific quantification. *NeuroImage*, 39(1), 336–347. <https://doi.org/10.1016/j.neuroimage.2007.07.053>
- Huang, Y., Bailey, S. K., Wang, P., Cutting, L. E., Gore, J. C., & Ding, Z. (2018). Voxel-wise detection of functional networks in white matter. *NeuroImage*, 183, 544–552.
- Hughes, A. J., Daniel, S. E., & Lees, A. J. (2001). Improved accuracy of clinical diagnosis of Lewy body Parkinson's disease. *Neurology*, 57(8), 1497–1499.
- Ji, G.-J., Liao, W., Chen, F.-F., Zhang, L., & Wang, K. (2017). Low-frequency blood oxygen level-dependent fluctuations in the brain white matter: More than just noise. *Science Bulletin*, 62(9), 656–657. <https://doi.org/10.1016/j.scib.2017.03.021>
- Ji, G. J., Liu, T., Li, Y., Liu, P., Sun, J., Chen, X., Tian, Y., Chen, X., Dahmani, L., Liu, H., Wang, K., & Hu, P. (2021). Structural correlates underlying accelerated magnetic stimulation in Parkinson's disease. *Human Brain Mapping*, 42(6), 1670–1681. <https://doi.org/10.1002/hbm.25319>
- Ji, G. J., Ren, C., Li, Y., Sun, J., Liu, T., Gao, Y., Xue, D., Shen, L., Cheng, W., Zhu, C., Tian, Y., Hu, P., Chen, X., & Wang, K. (2019). Regional and

- network properties of white matter function in Parkinson's disease. *Human Brain Mapping*, 40(4), 1253–1263. <https://doi.org/10.1002/hbm.24444>
- Jiang, Y., Luo, C., Li, X., Li, Y., Yang, H., Li, J., Chang, X., Li, H., Yang, H., Wang, J., Duan, M., & Yao, D. (2019). White-matter functional networks changes in patients with schizophrenia. *NeuroImage*, 190, 172–181. <https://doi.org/10.1016/j.neuroimage.2018.04.018>
- Jiang, Y., Song, L., Li, X., Zhang, Y., Chen, Y., Jiang, S., Hou, C., Yao, D., Wang, X., & Luo, C. (2019). Dysfunctional white-matter networks in medicated and unmedicated benign epilepsy with centrotemporal spikes. *Human Brain Mapping*, 40, 24584. <https://doi.org/10.1002/hbm.24584>
- Lanciego, J. L., Luquin, N., & Obeso, J. A. (2012). Functional neuroanatomy of the basal ganglia. *Cold Spring Harbor Perspectives in Medicine*, 2(12), a009621. <https://doi.org/10.1101/cshperspect.a009621>
- Lange, T., Roth, V., Braun, M. L., & Buhmann, J. M. (2004). Stability-based validation of clustering solutions. *Neural Computation*, 16(6), 1299–1323.
- Li, J., Biswal, B. B., Wang, P., Duan, X., Cui, Q., Chen, H., & Liao, W. (2019). Exploring the functional connectome in white matter. *Human Brain Mapping*, 40(15), 4331–4344. <https://doi.org/10.1002/hbm.24705>
- Li, M., Newton, A. T., Anderson, A. W., Ding, Z., & Gore, J. C. (2019). Characterization of the hemodynamic response function in white matter tracts for event-related fMRI. *Nature Communications*, 10(1), 1140. <https://doi.org/10.1038/s41467-019-09076-2>
- Li, R., Liao, W., Yu, Y., Chen, H., Guo, X., Tang, Y.-L., & Chen, H. (2018). Differential patterns of dynamic functional connectivity variability of striato-cortical circuitry in children with benign epilepsy with centrotemporal spikes. *Human Brain Mapping*, 39(3), 1207–1217.
- Liao, W., Ding, J., Marinazzo, D., Xu, Q., Wang, Z., Yuan, C., Zhang, Z., Lu, G., & Chen, H. (2011). Small-world directed networks in the human brain: Multivariate Granger causality analysis of resting-state fMRI. *NeuroImage*, 54(4), 2683–2694.
- Liao, W., Fan, Y.-S., Yang, S., Li, J., Duan, X., Cui, Q., & Chen, H. (2019). Preservation effect: Cigarette smoking acts on the dynamic of influences among unifying neuropsychiatric triple networks in schizophrenia. *Schizophrenia Bulletin*, 45(6), 1242–1250.
- Lorio, S., Fresard, S., Adaszewski, S., Kherif, F., Chowdhury, R., Frackowiak, R. S., Ashburner, J., Helms, G., Weiskopf, N., Lutti, A., & Draganski, B. (2016). New tissue priors for improved automated classification of subcortical brain structures on MRI. *NeuroImage*, 130, 157–166.
- Marussich, L., Lu, K.-H., Wen, H., & Liu, Z. (2017). Mapping white-matter functional organization at rest and during naturalistic visual perception. *NeuroImage*, 146, 1128–1141.
- Mišić, B., Fatima, Z., Askren, M. K., Buschkuhl, M., Churchill, N., Cimprich, B., Deldin, P. J., Jaeggi, S., Jung, M., Korostil, M., Kross, E., Krpan, K. M., Peltier, S., Reuter-Lorenz, P. A., Strother, S. C., Jonides, J., McIntosh, A. R., & Berman, M. G. (2014). The functional connectivity landscape of the human brain. *PLoS One*, 9(10), e111007.
- Mori, S., Wakana, S., Van Zijl, P. C., & Nagae-Poetscher, L. (2005). *MRI atlas of human white matter*. Elsevier.
- O'Malley, K. L. (2010). The role of axonopathy in Parkinson's disease. *Experimental Neurobiology*, 19(3), 115–119.
- Park, H.-J., & Friston, K. (2013). Structural and functional brain networks: From connections to cognition. *Science*, 342(6158), 1238411. <https://doi.org/10.1126/science.1238411>
- Pavese, N., & Brooks, D. J. (2009). Imaging neurodegeneration in Parkinson's disease. *Biochimica et Biophysica Acta (BBA)-Molecular Basis of Disease*, 1792(7), 722–729.
- Peer, M., Nitzan, M., Bick, A. S., Levin, N., & Arzy, S. (2017). Evidence for functional networks within the human brain's white matter. *The Journal of Neuroscience*, 37(27), 6394–6407. <https://doi.org/10.1523/JNEUROSCI.3872-16.2017>
- Pietracupa, S., Suppa, A., Upadhyay, N., Gianni, C., Grillea, G., Leodori, G., Modugno, N., di Biasio, F., Zampogna, A., Colonnese, C., Berardelli, A., & Pantano, P. (2018). Freezing of gait in Parkinson's disease: Gray and white matter abnormalities. *Journal of Neurology*, 265(1), 52–62. <https://doi.org/10.1007/s00415-017-8654-1>
- Poewe, W., Seppi, K., Tanner, C. M., Halliday, G. M., Brundin, P., Volkman, J., Schrag, A. E., & Lang, A. E. (2017). Parkinson disease. *Nature Reviews Disease Primers*, 3(1), 1–21. <https://doi.org/10.1038/nrdp.2017.13>
- Power, J. D., Barnes, K. A., Snyder, A. Z., Schlaggar, B. L., & Petersen, S. E. (2012). Spurious but systematic correlations in functional connectivity MRI networks arise from subject motion. *NeuroImage*, 59(3), 2142–2154.
- Rodríguez-Herreros, B., Amengual, J. L., Gurtubay-Antolín, A., Richter, L., Jauer, P., Erdmann, C., Schweikard, A., López-Moliner, J., Rodríguez-Fornells, A., & Münte, T. F. (2015). Microstructure of the superior longitudinal fasciculus predicts stimulation-induced interference with on-line motor control. *NeuroImage*, 120, 254–265. <https://doi.org/10.1016/j.neuroimage.2015.06.070>
- Salvador, R., Suckling, J., Coleman, M. R., Pickard, J. D., Menon, D., & Bullmore, E. (2005). Neurophysiological architecture of functional magnetic resonance images of human brain. *Cerebral Cortex*, 15(9), 1332–1342.
- Sanjari Moghaddam, H., Dolatshahi, M., Mohebi, F., & Aarabi, M. H. (2020). Structural white matter alterations as compensatory mechanisms in Parkinson's disease: A systematic review of diffusion tensor imaging studies. *Journal of Neuroscience Research*, 98(7), 1398–1416. <https://doi.org/10.1002/jnr.24617>
- Schwarzkopf, D. S., De Haas, B., & Rees, G. (2012). Better ways to improve standards in brain-behavior correlation analysis. *Frontiers in Human Neuroscience*, 6, 200. <https://doi.org/10.3389/fnhum.2012.00200>
- Tagliaferro, P., Kareva, T., Oo, T. F., Yarygina, O., Kholodilov, N., & Burke, R. E. (2015). An early axonopathy in a hLRRK2 (R1441G) transgenic model of Parkinson disease. *Neurobiology of Disease*, 82, 359–371.
- Thomas Yeo, B. T., Krienen, F. M., Sepulcre, J., Sabuncu, M. R., Lashkari, D., Hollinshead, M., Roffman, J. L., Smoller, J. W., Zöllei, L., Polimeni, J. R., Fischl, B., Liu, H., & Buckner, R. L. (2011). The organization of the human cerebral cortex estimated by intrinsic functional connectivity. *Journal of Neurophysiology*, 106(3), 1125–1165. <https://doi.org/10.1152/jn.00338.2011>
- Tomlinson, C. L., Stowe, R., Patel, S., Rick, C., Gray, R., & Clarke, C. E. (2010). Systematic review of levodopa dose equivalency reporting in Parkinson's disease. *Movement Disorders*, 25(15), 2649–2653. <https://doi.org/10.1002/mds.23429>
- Tong, Y., Lindsey, K. P., Hocke, L. M., Vitaliano, G., Mintzopoulos, D., & Frederick, B. D. (2017). Perfusion information extracted from resting state functional magnetic resonance imaging. *Journal of Cerebral Blood Flow & Metabolism*, 37(2), 564–576. <https://doi.org/10.1177/0271678X16631755>
- Wang, X., Yoo, K., Chen, H., Zou, T., Wang, H., Gao, Q., Meng, L., Hu, X., & Li, R. (2022). Antagonistic network signature of motor function in Parkinson's disease revealed by connectome-based predictive modeling. *Npj Parkinsons Disease*, 8(1), 49. <https://doi.org/10.1038/s41531-022-00315-w>
- Wen, M.-C., Heng, H. S., Lu, Z., Xu, Z., Chan, L. L., Tan, E. K., & Tan, L. C. (2018). Differential white matter regional alterations in motor subtypes of early drug-naive Parkinson's disease patients. *Neurorehabilitation and Neural Repair*, 32(2), 129–141.
- Wen, M.-C., Heng, H. S., Ng, S. Y., Tan, L. C., Chan, L. L., & Tan, E. K. (2016). White matter microstructural characteristics in newly diagnosed Parkinson's disease: An unbiased whole-brain study. *Scientific Reports*, 6(1), 1–9.
- Wolters, A. F., van de Weijer, S. C. F., Leentjens, A. F. G., Duits, A. A., Jacobs, H. I. L., & Kuijf, M. L. (2019). Resting-state fMRI in Parkinson's disease patients with cognitive impairment: A meta-analysis.

Parkinsonism & Related Disorders, 62, 16–27. <https://doi.org/10.1016/j.parkreldis.2018.12.016>

- Wonderlick, J., Ziegler, D. A., Hosseini-Varnamkhasti, P., Locascio, J., Bakkour, A., Van Der Kouwe, A., Triantafillou, C., Corkin, S., & Dickerson, B. C. (2009). Reliability of MRI-derived cortical and subcortical morphometric measures: Effects of pulse sequence, voxel geometry, and parallel imaging. *NeuroImage*, 44(4), 1324–1333.
- Wu, X., Yang, Z., Bailey, S. K., Zhou, J., Cutting, L. E., Gore, J. C., & Ding, Z. (2017). Functional connectivity and activity of white matter in somatosensory pathways under tactile stimulations. *NeuroImage*, 152, 371–380.
- Zhao, Y., Zhang, F., Zhang, W., Chen, L., Chen, Z., Lui, S., & Gong, Q. (2021). Decoupling of gray and white matter functional networks in medication-naïve patients with major depressive disorder. *Journal of Magnetic Resonance Imaging*, 53(3), 742–752.

SUPPORTING INFORMATION

Additional supporting information may be found in the online version of the article at the publisher's website.

How to cite this article: Meng, L., Wang, H., Zou, T., Wang, X., Chen, H., Xie, F., & Li, R. (2022). Attenuated brain white matter functional network interactions in Parkinson's disease. *Human Brain Mapping*, 43(15), 4567–4579. <https://doi.org/10.1002/hbm.25973>